Observation of resonance fluorescence and the Mollow triplet from a coherently driven site-controlled quantum dot

Unsleber, Sebastian; Maier, Sebastian; McCutcheon, Dara; He, Yu-Ming; Dambach, Michael; Gschrey, Manuel; Gregersen, Niels; Mørk, Jesper; Reitzenstein, Stephan; Höfling, Sven

Total number of authors:
12

Published in:
Optica

Link to article, DOI:
10.1364/optica.2.001072

Publication date:
2015

Document Version
Publisher's PDF, also known as Version of record

optica

Observation of resonance fluorescence and the Mollow triplet from a coherently driven site-controlled quantum dot

Sebastian Unsleber,[1,†] Sebastian Maier,[1,†] Dara P. S. McCutcheon,[2] Yu-Ming He,[1,3] Michael Dambach,[1] Manuel Gschrey,[4] Niels Gregersen,[2] Jesper Mørk,[2] Stephan Reitzenstein,[4] Sven Höfling,[1,3,5] Christian Schneider,[1,*] and Martin Kamp[1]

[1]Technische Physik and Wilhelm Conrad Röntgen Research Center for Complex Material Systems, Physikalisches Institut, Universität Würzburg, Am Hubland, D-97074 Würzburg, Germany
[2]Department of Photonics Engineering, Technical University of Denmark, Ørsteds Plads, 2800 Kgs. Lyngby, Denmark
[3]Hefei National Laboratory for Physical Sciences at the Microscale and Department of Modern Physics, and CAS Center for Excellence and Synergetic Innovation Center in Quantum Information and Quantum Physics, University of Science and Technology of China, Hefei, Anhui 230026, China
[4]Institut für Festkörperphysik, Technische Universität Berlin, Hardenbergstraße 36, 10623 Berlin, Germany
[5]SUPA, School of Physics and Astronomy, University of St Andrews, St Andrews, KY16 9SS, UK
*Corresponding author: christian.schneider@physik.uni-wuerzburg.de

Received 28 July 2015; revised 6 November 2015; accepted 7 November 2015 (Doc. ID 246966); published 16 December 2015

Resonant excitation of solid state quantum emitters has the potential to deterministically excite a localized exciton while ensuring maximally coherent emission. In this work, we demonstrate the coherent coupling of an exciton localized in a lithographically positioned, site-controlled semiconductor quantum dot to an external resonant laser field. For strong continuous-wave driving we observe the characteristic Mollow triplet and analyze the Rabi splitting and sideband widths as a function of driving strength and temperature. The sideband widths increase linearly with temperature and the square of the driving strength, which we explain via coupling of the exciton to longitudinal acoustic phonons. We also find an increase of the Rabi splitting with temperature, which indicates a temperature-induced delocalization of the excitonic wave function resulting in an increase of the oscillator strength. Finally, we demonstrate coherent control of the exciton excited state population via pulsed resonant excitation and observe a damping of the Rabi oscillations with increasing pulse area, which is consistent with our exciton–photon coupling model. We believe that our work outlines the possibility to implement fully scalable platforms of solid state quantum emitters. Such scalability is one of the key prerequisites for more advanced, integrated nanophotonic quantum circuits.

OCIS codes: (230.5590) Quantum-well, -wire and -dot devices; (220.4241) Nanostructure fabrication; (270.0270) Quantum optics; (300.6470) Spectroscopy, semiconductors.

http://dx.doi.org/10.1364/OPTICA.2.001072

1. INTRODUCTION

Semiconductor self-assembled quantum dots (QDs) are prime candidates for solid state quantum emitters [1,2]. Many groundbreaking experiments have shown their great potential, e.g., in quantum key distribution experiments [3,4], the demonstration of spin–photon entanglement [5,6], and the emission of highly indistinguishable single photons [7,8]. Furthermore, quantum dots offer advantages compared to alternative platforms, e.g., cold atoms or trapped ions, such as their ability to be electrically contacted [9–11], and the possibility to be implemented into photonic architectures or networks [12–14].

Thus far, most relevant demonstrations were carried out based on randomly positioned QDs. Scalable schemes for the implementation of solid state quantum bits or quantum emitters, however, require position control over the QDs. This has triggered extensive research activities to realize site-controlled QD (SCQD) arrays [15–17]. While single photon emission [18,19] and the emission of indistinguishable [20] and polarization entangled photons [21] in this system have been demonstrated, the implementation of resonant fluorescence in this system remains elusive. Resonant coupling of a laser to the quantum emitter, however, is key toward the emission of single photons with high indistinguishability and to coherently control the state of the excitonic qubit. In this work, we demonstrate for the first time, to the best of our knowledge, the resonant excitation of a SCQD. We observe the characteristic Mollow triplet [22–24] in the resonance fluorescence spectra under continuous-wave excitation conditions, and demonstrate the coherent control of the excited

state SCQD population via pulsed resonant excitation. Furthermore, we analyze the light–matter coupling for varying temperatures and driving strengths, which allows us to characterize the strength of exciton–phonon interactions and assess the lateral exciton extension in the quantum dot.

2. SAMPLE STRUCTURE AND SETUP

Our sample consists of stacked site-controlled InAs quantum dots that are embedded in a single-sided planar cavity to improve the light extraction, as shown in Fig. 1(a). After the growth of the bottom distributed Bragg reflector (DBR) with 30 quarter-wavelength thick AlAs/GaAs mirror pairs and a 85 nm thick GaAs layer via molecular beam epitaxy, arrays of nanoholes with a 2 μm pitch are defined on the wafer by means of electron beam lithography and wet-chemical etching [17]. The structure design in principle allows us to yield photon extraction efficiencies on the order of ≈10–12% [25] for the microscope objective with NA = 0.42 that we used. We note that this number can be further increased by utilizing micropillar cavities (based on devices with top DBR [7,19,26]), or by shaping the confinement in broadband approaches via dielectric lenses [27–29]. The prepatterned sample is deoxidized with thermally activated hydrogen before the second epitaxial growth step is performed. The nanoholes are then capped by 10 nm GaAs and a first InAs quantum dot layer (seeding layer) at a substrate temperature of 540°C to maximize the migration length and to ensure that nucleation preferentially takes place in the nanoholes. To improve the optical quality of the quantum dots, a second layer of InAs quantum dots is separated by a 35 nm thick GaAs separation layer, while the positioning of the SCQDs is maintained by the vertical strain field [Fig. 1(b)]. In Fig. 1(c) a scanning electron microscopy (SEM) image shows SCQDs with a 2 μm period on an uncapped reference sample, recorded under an angle of 70° to enhance the imaging contrast. The emission wavelength range of the buried QDs in our device is shifted toward 900 nm by performing an *in situ* annealing step, before a 131 nm thick GaAs layer completes the structure. A titanium grid on the surface of the sample with a pitch of 12 μm and 300 nm width [Fig. 1(a)] is defined by means of e-beam lithography. This serves as a coordinate system for orientation, with each grid square containing a regular array of 36 SCQDs.

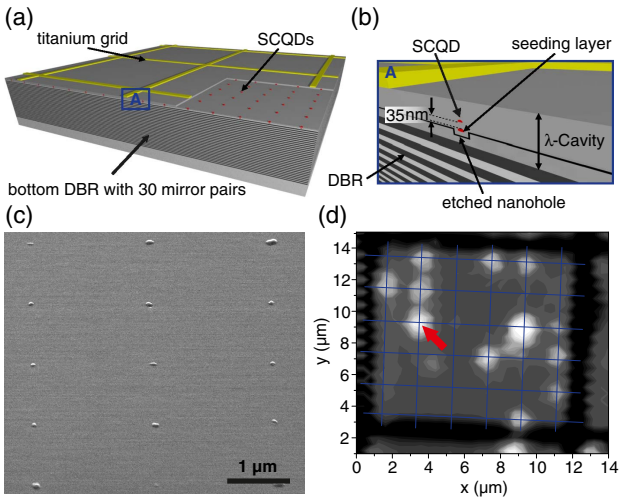

Fig. 1. (a) Schematic drawing of the sample structure showing the lower DBR and the λ-thick spacer with embedded SCQDs. (b) Detailed layer sequence with two quantum dot layers and the 35 nm thick GaAs separation layer in between. (c) SEM image of SCQDs on an uncapped calibration sample. (d) μPL-map of a 14 μm × 14 μm area. The bright spots are SCQDs that are located on a 2 μm grid that was predefined by nanoholes. The blue grid serves as a guide to the eye; the red arrow indicates the SCQD that is subject to the in-depth study.

The sample is mounted on the cold-finger of a He flow cryostat and is excited by a continuous-wave laser at 532 nm. Figure 1(d) shows a 14 μm × 14 μm large array scan of the photoluminescence (PL) signal of the sample. The bright spots between the titanium frames can be attributed to the PL signal of SCQDs that are located on the expected positions of the array. SEM images of the uncapped sample shown in Fig. 1(c) indicate that SCQDs are present at all expected positions. As such, we attribute dark spots on the grid to a large variation in quantum efficiencies [30]. The SCQD indicated with a red arrow in Fig. 1(d) is the basis of detailed subsequent μPL investigations. The QD is excited by either a fiber coupled continuous-wave diode laser or a pulsed Ti:sapphire laser with a repetition rate of $f = 82$ MHz and a pulse length of $\Delta t \approx 1.2$ ps. In order to suppress the resonant laser, we use a cross-polarization configuration where the excitation laser and the detected SCQD signal have perpendicular polarizations. The emitted photons are then analyzed via a double monochromator with two 1200 lines/mm gratings and a nitrogen cooled Si-CCD ($\Delta E_{\mathrm{Res}} \approx 20$ μeV).

3. THEORY

For the interpretation of our experimental results, we employ basic concepts of the theory of a resonantly driven quantum dot coupled to longitudinal acoustic (LA) phonons. In Ref. [31] it was shown that provided $\Omega < k_B T < \omega_c$, with Ω the Rabi frequency, k_B the Boltzmann constant, T the sample temperature, and ω_c the cut-off frequency of the phonon environment, the effect of phonons on the excitonic dynamics can be accurately captured by a renormalization of the bare Rabi frequency and the introduction of a phonon-induced pure-dephasing rate. We write the optical Bloch equations describing the excitonic degrees of freedom as

$$\dot{\alpha}_x = -\Gamma_2 \alpha_x, \tag{1}$$

$$\dot{\alpha}_y = -\Gamma_2 \alpha_y - \Omega_r \alpha_z, \tag{2}$$

$$\dot{\alpha}_z = -\Gamma_1 \alpha_z + \Omega_r \alpha_z - \Gamma_1, \tag{3}$$

where $\alpha_i = \langle \sigma_i \rangle = \mathrm{Tr}(\rho \sigma_i)$ for $i = x, y, z$ and ρ the exciton density operator, and we work in a basis where $\sigma_x = |e\rangle\langle g| + |g\rangle\langle e|$, $\sigma_y = -i|e\rangle\langle g| + i|g\rangle\langle e|$, and $\sigma_z = |e\rangle\langle e| - |g\rangle\langle g|$ with $|e\rangle$ and $|g\rangle$ being the single exciton and ground states, respectively. The total dephasing rate is given by $\Gamma_2 = \frac{1}{2}\Gamma_1 + \gamma_{\mathrm{PD}} + \gamma_0$, where $\Gamma_1 = 1/T_1$ is the spontaneous emission rate, γ_0 captures dephasing not attributed to phonons, and γ_{PD} is the phonon-induced dephasing rate, which we define below. The effective Rabi frequency is given by (for $\hbar = 1$)

$$\Omega_r = \mu E_0 R \,(= \kappa \sqrt{P}), \tag{4}$$

with μ the dipole moment of the emitter, E_0 the electric field strength of the laser light, R a phonon-induced renormalization factor, κ representing the product μR, and P the laser power.

Exciton–phonon coupling is characterized by the spectral density, which for coupling to LA phonons takes the form

$J(\omega) = \alpha\omega^3 \exp[-(\omega/\omega_c)^2]$, with α capturing the overall strength of the interaction [32,33]. In terms of the spectral density, the phonon-induced renormalization factor is given by [31,34,35]

$$R = \exp\left[-\frac{1}{2}\int_0^\infty d\omega \frac{J(\omega)}{\omega^2} \coth(\omega/2k_BT)\right]. \quad (5)$$

In the weak exciton–phonon coupling limit, the phonon-induced pure-dephasing rate is given by

$$\gamma_{PD} = (\pi/2)J(\Omega_r)\coth(\Omega_r/2k_BT), \quad (6)$$

which becomes

$$\gamma_{PD} = \pi\alpha k_B T\Omega_r^2 \ (= \chi\Omega_r^2), \quad (7)$$

provided $\Omega_r \ll k_BT$, ω_c and χ being the product $\pi\alpha k_BT$. We note that this last condition is typically met in continuous-wave measurements due to the relatively small Rabi frequencies. For pulsed measurements, however, instantaneous Rabi frequencies can reach levels comparable to ω_c, $k_BT \sim 1$meV (at $T = 10$ K). In the following, we therefore use the simpler expression given in Eq. (7) for the continuous-wave measurements, but the full expression in Eq. (6) when investigating pulsed excitation conditions.

The incoherent component of the resonance fluorescence spectrum is given by $S(\omega)\propto\mathrm{Re}[\int_0^\infty d\tau(g^{(1)}(\tau)-g^{(1)}(\infty))\exp[-i\omega\tau]]$, where $g^{(1)}(\tau)=\lim_{t\to\infty}\langle\sigma^\dagger(t+\tau)\sigma(t)\rangle$ with $\sigma = |g\rangle\langle e|$ being the steady-state first-order field correlation function. From Eqs. (1)–(3), calculation of the field correlation function and fluorescence spectrum proceeds by invoking the quantum regression theorem [36,37]. It is found that above saturation ($\Omega_r \gg \Gamma_1$), the fluorescence spectrum consists of three Lorentzian peaks, one centered at the laser driving frequency, and two more positioned on either side at a distance of Ω_r. In this regime the full width at half-maximum (FWHM) of the sidebands is given by [35]

$$\Delta\omega = \frac{3}{2}\Gamma_1 + \gamma_{PD} + \gamma_0. \quad (8)$$

From these expressions we see that we expect the sideband widths to increase linearly with Ω_r^2, with an intersect (as $\Omega_r \to 0$) given by $(3/2)\Gamma_1 + \gamma_0$. Moreover, since $E_0 \sim \sqrt{P}$, for constant μ one expects the gradient $(d\Omega_r/d\sqrt{P}) \sim \mu R$ to decrease with temperature since R decreases, as was experimentally observed in Ref. [35].

4. EXPERIMENTAL RESULTS AND ANALYSIS

First, we study the emission properties of the SCQD under pulsed nonresonant excitation. To do so, we couple the spectrally filtered microphotoluminescence emission into a fiber-based Hanbury Brown and Twiss setup in order to measure the second-order autocorrelation function. A histogram of coincidence events measured as a function of detection time delay is shown in Fig. 2(a). The suppressed peak around $\tau \approx 0$ ns is a clear signature for single photon emission from our SCQD. We extract a $g^{(2)}(0)$ value by dividing the area of the central peak by the average area of the surrounding peaks, which yields a value of $g^{(2)}(0) = 0.39 \pm 0.02$ (corrected according to [38] by spectral background emission $g^{(2)}(0) = 0.22 \pm 0.02$). Remaining two-photon detection events arise from refilling of the SCQD due to the nonresonant excitation. In addtition, fitting the sidepeaks with a two-sided exponential function allows us to extract the lifetime of the exciton, and we find $T_1 = (561 \pm 68)$ ps. Compared to standard

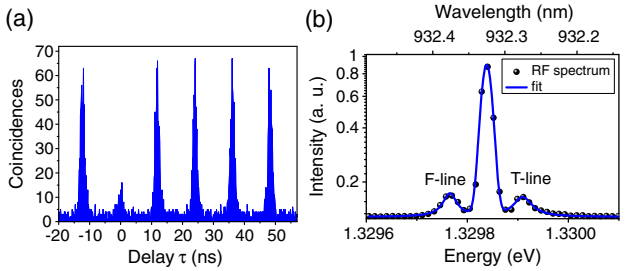

Fig. 2. (a) Second-order autocorrelation function for pulsed nonresonant excitation and a sample temperature of $T = 6.8$ K. We extract a $g^{(2)}(0)$ value of $g^{(2)}(0) = 0.39 \pm 0.02$. (b) Resonance fluorescence (RF) spectrum of a SCQD for a pump power of $P = 746$ nW at $T = 5$ K. The triplet peak structure is a signature of coherent coupling between the quantum dot exciton and the laser field.

In(Ga)As QDs grown under comparable conditions [39], the T_1 time is slightly reduced. We believe this is a consequence of the presence of nonradiative recombination channels that play a significant role for QDs grown on patterned substrates [30].

Next, we study the SCQD's emission properties under strict resonant excitation. Therefore, we drive the single exciton transition on resonance with a continuous-wave laser, and analyze the spectrum of the emitted radiation. Figure 2(b) shows a representative spectrum of resonance fluorescence from the investigated SCQD corresponding to a pump power of $P = 746$ nW and at a temperature of $T = 5$ K. Due to imperfections of the sample surface the laser is not fully suppressed, resulting in a ratio of the sidepeak area to the central peak of approximately 1:12. We fit the spectrum to a sum of two Lorenztians for the sidepeaks and a Gaussian for the central peak, which is resolution limited. From the fit, for this pump power and temperature we obtain sidepeak widths of $\Delta\omega_F = (31 \pm 7)$ μeV and $\Delta\omega_T = (43 \pm 9)$ μeV and a Rabi splitting of $\Omega_r = 72$ μeV.

For increasing pump power but at fixed temperature, the sidepeak splitting increases as predicted by theory. Figure 3(a) shows this splitting as a function of the square root of the laser power. The splitting follows a clear linear dependence, as is expected from Eq. (4) and recalling that the field amplitude $E_0 \propto \sqrt{P}$ [24]. From the fits, we obtain a slope of $\kappa = \pm(5.04 \pm 0.01)$ μeV/$\sqrt{\mu W}$, which is slightly smaller than it is reported for self-organized QDs ([35]: $\kappa = 7.6$ μeV/$\sqrt{\mu W}$). Figure 3(b) shows

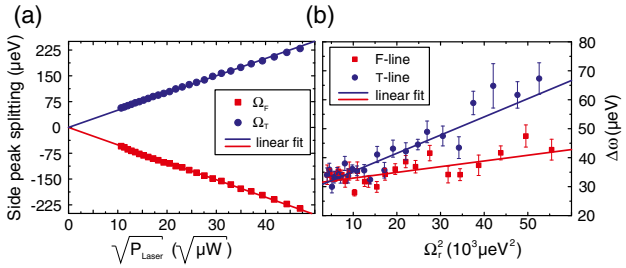

Fig. 3. (a) Rabi splitting as a function of the square root of the pump power at $T = 5$ K. A clear linear increase is observed with effective dipole moment of $\kappa = \pm(5.04 \pm 0.01)\frac{\mu eV}{\sqrt{\mu W}}$. (b) Linewidth of the Mollow sidepeaks as a function of the Rabi frequency. A linear trend is consistent with Eq. (7), suggesting dephasing caused by coupling to LA phonons.

the variation of the sideband linewidths as a function of the square of the Rabi frequency. We observe a linear behavior with gradients of $\chi_F = (2.0 \pm 0.6) \cdot 10^{-4}$ μeV^{-1} for the F line and $\chi_T = (6.3 \pm 0.7) \cdot 10^{-4}$ μeV^{-1} for the T line. The linear behavior is consistent with Eq. (7), suggesting excitation-induced dephasing caused by coupling to LA phonons in our sample. Additionally, from Eq. (8) we see that the intersects with the y axis give non-phonon-induced dephasing rates of $\gamma_0 \approx 30$ μeV. We note that for resonant excitation, our theory predicts F and T sidebands of equal width. We attribute the systematic asymmetry to a slight detuning of the QD level from the excitation laser, which becomes more pronounced at the high pump powers we use in order to maximize the Rabi splitting. Such asymmetries have been predicted in [40] for systems with relatively high dephasing rates, and arise as a result of the exciton–phonon coupling interaction, producing behavior that departs from a simple pure-dephasing model. The larger broadening of the T line seen in our measurements suggests that our laser is blue shifted from the QD transition. A systematic investigation of these off-resonance effects and their underlying physical mechanisms has yet to be performed, and this is a topic that we plan to explore fully in future work.

To further characterize our system, we performed measurements of the sidepeak splitting and linewidth for temperatures up to 35 K. In Fig. 4(a) we plot χ [see Eq. (7)] as a function of the sample temperature. χ is the parameter that captures the broadening of the Mollow sidepeaks. We observe a monotonous increase of χ with the sample temperature, and by fitting to Eq. (7) we can extract $\alpha_F = (0.077 \pm 0.015)$ ps^2 and $\alpha_T = (0.113 \pm 0.012)$ ps^2, which are consistent with other experiments carried out on standard In(Ga)As QDs [32,33,35]. The solid lines in Fig. 4(a) show $\gamma_{PD}/\Omega_r^2 = \pi\alpha k_B T$ using these extracted values. We attribute the slight scattering of the datapoints to a slight detuning caused by the high driving strength we used in the experiment. As mentioned above, the power dephasing coefficient is a sensitive function to the laser detuning, which we cannot exclude to slightly change during the experiment.

Figure 4(b) shows the renormalized dipole moment $\kappa = \mu R$ [see Eq. (4)] as the temperature is increased. We first obtain a decrease in the effective dipole moment for temperatures up to 15 K, followed by a clear increase for higher temperatures. From Eq. (4), we read $d\Omega_r/d\sqrt{P} \propto \mu R$. Since the phonon renormalization parameter R decreases with rising temperature, one also expects a decrease of $d\Omega_r/d\sqrt{P}$ with temperature. This is what we observe for $T < 15$ K. Above 15 K, the notable increase suggests an increase in the dipole moment μ with temperature. We assume that the indium concentration in our QD is nonuniform, which leads to shallow potential minimums within the QD that trap the exciton at very low temperatures. Once a characteristic activation energy is thermally overcome, the exciton wave function spreads over the entire QD, leading to an increase of the dipole moment μ, and thus to a stronger coupling to the resonant laser field. Similar observations were found via magneto-optical studies on self-assembled QDs [41].

For potential applications of our SCQDs, it is desirable that the excited state population can be coherently controlled, which we now demonstrate using pulsed resonant excitation. Figure 5(a) shows the emission spectrum of the same SCQD under pulsed resonant excitation ($f_{Rep} = 82$ MHz, $\Delta t \approx 1.2$ ps). A broad remaining laser background is observed due to the temporally narrow excitation pulses. To extract the quantum dot emission intensity, we fit the QD emission in each single spectrum with a Gaussian function and extract the integrated intensity from the fit results.

The results are shown in Fig. 5(b), where a damped sinusoidal behavior is observed. This is consistent with our exciton–phonon coupling model, which [according to Eq. (7)] predicts an increase in dephasing for larger pulse strengths, and has been observed elsewhere for conventional, self assembled QDs [32–34]. In fact, we can use Eqs. (1)–(3) to fit the experimentally measured intensities as a function of pulse area. The integrated emission intensity is proportional to the final excited state population, which we can simulate using the optical Bloch equations. To do so, we make the replacement $\Omega_r \to R(\Theta/2\tau\sqrt{\pi}) \exp[-(t/2\tau)^2]$, with $\tau = \Delta t/4\sqrt{\ln 2}$, Θ being the pulse area, and we set $\Gamma_1 = 0$ since we are interested in timescales of the order $\Delta t \ll T_1$. We then numerically solve Eqs. (1)–(3) using the full phonon-induced pure-dephasing rate in Eq. (6) for each excitation power, allowing for a scaling factor between $\sqrt{P_{laser}}$ and Θ, fixing $\gamma_0 = 30$ μeV from our previous fits, and allowing the exciton–phonon coupling parameter α and the cut-off frequency ω_c to vary.

The result of this fitting procedure is shown by the solid line in Fig. 5(b), and the exciton–phonon coupling parameters we extract are $\alpha = (0.054 \pm 0.016)$ ps^2 and $\omega_c = (4.34 \pm 1.21)$ ps^{-1}.

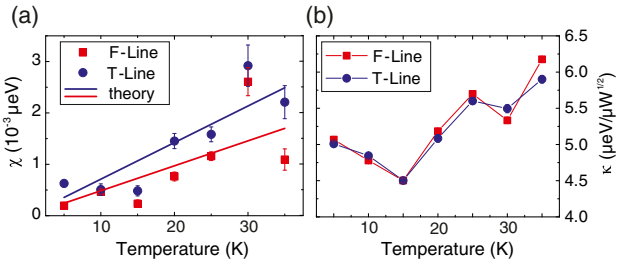

Fig. 4. (a) Change in the Mollow sideband widths with squared Rabi frequency as a function of temperature. The lines show a fitting to the exciton–phonon coupling model. (b) Gradient of the renormalized Rabi splitting with increasing pump power versus the temperature. We observe a notable increase for temperatures exceeding 15 K, which is attributed to a localization effect of the excitonic wave function for low temperatures.

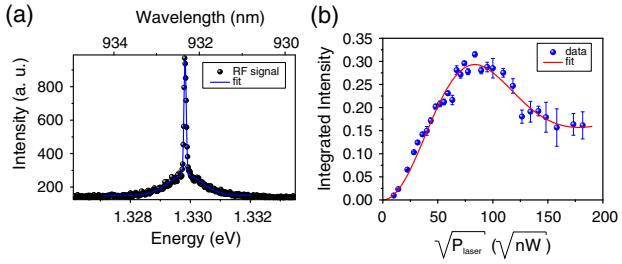

Fig. 5. (a) Quantum dot spectrum under pulsed resonant excitation and for a sample temperature of $T = 5.8$ K. The fit is a double Gaussian function for the dot emission and the remaining laser background. (b) Integrated intensity of the quantum dot emission as a function of the square root of the pump power. The intensity is obtained from fitting the single spectra. The solid line is a fit to theory including coupling to phonons.

We see that our model is able to capture the experimental data well, though the exciton–phonon coupling strength α that we extract differs slightly from those found for continuous-wave driving. There are a number of possible reasons for this discrepancy. First, we note that similarly good fits can be found in the pulsed excitation case by fixing α to a value closer to that found for continuous driving, and allowing instead the background dephasing rate γ_0 to vary. As such, in the case of pulsed excitation it is not straightforward to distinguish phonon-induced dephasing from other sources. We also note that while the fundamental exciton–phonon coupling parameters α and ω_c should not depend on the excitation scheme, the background rate γ_0 may well differ in the two cases, particularly for temporally short pulses that have spectral components that are not resonant with the exciton transition energy [8]. Finally, we note that replacing the Rabi frequency Ω_r in Eq. (6) with a time-dependent quantity requires making a Markovian approximation, which assumes the phonon environment relaxes on a timescale shorter than the excitonic dynamics [33,34]. For the short temporal pulses used here this approximation may not be strictly valid, and we note that it will be interesting to explore potential non-Markovian effects in these systems in future works [37].

5. SUMMARY

We have shown for the first time, to the best of our knowledge, the coherent coupling of a resonant laser field to the excitonic state of a SCQD. We observed the characteristic Mollow triplet in the spectral domain and an increase in the Rabi splitting with increasing temperature, which we attribute to a localization of the SCQD wave function for low temperatures due to a gradient in the indium concentration inside the SCQD. Furthermore, we analyzed in detail the power and temperature-dependent dephasing channels in our system. Finally, we demonstrate the coupling of the QD exciton to a pulsed resonant laser field by measuring the dependency of the SCQD emission on the pulse area of the excitation laser. The observed Rabi oscillations feature a distinct damping, which points toward the presence of exciton–phonon coupling in our system. The possibility to generate resonance fluorescence photons from positioned quantum dots opens new experimental opportunities for realizing scalable solid state quantum emitters. This is a crucial step toward the deterministic generation of single photons with unity indistinguishability [7], and resonant techniques are key for obtaining optical coherent control over single spins in QDs [42]. The implementation of such schemes, based on a fully scalable quantum emitter architecture (such as provided by SCQDs), remains one of the big challenges in solid state quantum emitter research. As a next step toward this architecture, an implementation of SCQDs within microcavities is desirable. Due to the control over the nucleation spot, one can expect an almost perfect coupling of the SCQD to the fundamental optical mode of such a device that gives rise to increased extraction efficiencies and high degrees of indistinguishability, which is key for realizing an efficient source of indistinguishable photons.

Funding. Bundesministerium für Bildung und Forschung (BMBF) (Q.com-HL); CHIST-ERA (SSQN); Deutsche Forschungsgemeinschaft (DFG Ka2318/4-1, SFB 787); Deutscher Akademischer Austauschdienst (DAAD) (CSC-DAAD Postdoc Scholarship Program); European Metrology Research Programme (EMRP) (SIQUTE (EXL02)); Royal Society (Wolfson Foundation); Villum Fonden.

Acknowledgment. The authors thank M. Emmerling for sample preparation. This work was funded by project SIQUTE (contract EXL02) of the European Metrology Research Programme (EMRP). The EMRP is jointly funded by the EMRP participating countries within EURAMET and the European Union. Support was provided from the Villum Foundation via the VKR Centre of Excellence NATEC.

†These authors contributed equally.

REFERENCES

1. P. Michler, A. Kiraz, C. Becher, W. V. Schoenfeld, P. M. Petroff, L. Zhang, E. Hu, and A. Imamoglu, "A quantum dot single-photon turnstile device," Science **290**, 2282–2285 (2000).
2. C. Santori, D. Fattal, J. Vuckovic, G. S. Solomon, and Y. Yamamoto, "Indistinguishable photons from a single-photon device," Nature **419**, 594–597 (2002).
3. E. Waks, K. Inoue, C. Santori, D. Fattal, J. Vuckovic, G. S. Solomon, and Y. Yamamoto, "Quantum cryptography with a photon turnstile," Nature **420**, 762 (2002).
4. T. Heindel, C. A. Kessler, M. Rau, C. Schneider, M. Fürst, F. Hargart, W.-M. Schulz, M. Eichfelder, R. Rossbach, S. Nauerth, M. Lermer, H. Weier, M. Jetter, M. Kamp, S. Reitzenstein, S. Höfling, P. Michler, H. Weinfurter, and A. Forchel, "Quantum key distribution using quantum dot single-photon emitting diodes in the red and near infrared spectral range," New J. Phys. **14**, 083001 (2012).
5. K. De Greve, L. Yu, P. L. McMahon, J. S. Pelc, C. M. Natarajan, N. Y. Kim, E. Abe, S. Maier, C. Schneider, M. Kamp, S. Höfling, R. H. Hadfield, A. Forchel, M. M. Fejer, and Y. Yamamoto, "Quantum-dot spin-photon entanglement via frequency downconversion to telecom wavelength," Nature **491**, 421–425 (2012).
6. W. B. Gao, P. Fallahi, E. Togan, J. Miguel-Sanchez, and A. Imamoglu, "Observation of entanglement between a quantum dot spin and a single photon," Nature **491**, 426–430 (2012).
7. Y.-M. He, Y. He, Y.-J. Wei, D. Wu, M. Atatüre, C. Schneider, S. Höfling, M. Kamp, C.-Y. Lu, and J.-W. Pan, "On-demand semiconductor single-photon source with near-unity indistinguishability," Nat. Nanotechnol. **8**, 213–217 (2013).
8. Y.-J. Wei, Y.-M. He, M.-C. Chen, Y.-N. Hu, Y. He, D. Wu, C. Schneider, M. Kamp, S. Höfling, C.-Y. Lu, and J.-W. Pan, "Deterministic and robust generation of single photons from a single quantum dot with 99.5% indistinguishability using adiabatic rapid passage," Nano Lett. **14**, 6515–6519 (2014).
9. T. Heindel, C. Schneider, M. Lermer, S. H. Kwon, T. Braun, S. Reitzenstein, S. Höfling, M. Kamp, and A. Forchel, "Electically driven quantum dot-micropillar single photon source with 34% overall efficiency," Appl. Phys. Lett. **96**, 011107 (2010).
10. D. J. P. Ellis, A. J. Bennett, S. J. Dewhurst, C. A. Nicoll, D. A. Ritchie, and A. J. Shields, "Cavity-enhanced radiative emission rate in a single-photon-emitting diode operating at 0.5 GHz," New J. Phys. **10**, 043035 (2008).
11. Z. Yuan, B. E. Kardynal, R. M. Stevenson, A. J. Shields, C. J. Lobo, K. Cooper, N. S. Beattie, D. A. Ritchie, and M. Pepper, "Electrically driven single-photon source," Science **295**, 102–105 (2002).
12. T. B. Hoang, J. Beetz, M. Lermer, L. Midolo, M. Kamp, S. Höfling, and A. Fiore, "Widely tunable, efficient on-chip single photon sources at telecommunication wavelengths," Opt. Express **20**, 21758–21765 (2012).
13. P. Yao, V. S. C. M. Rao, and S. Hughes, "On-chip single photon sources using planar photonic crystals and single quantum dots," Laser Photon. Rev. **4**, 499–516 (2010).
14. K. D. Jöns, U. Rengstl, M. Oster, F. Hargart, M. Heldmaier, S. Bounouar, S. M. Ulrich, M. Jetter, and P. Michler, "Monolithic on-chip integration of semiconductor waveguides, beamsplitters and single-photon sources," J. Phys. D **48**, 085101 (2015).

15. T. Ishikawa, T. Nishimura, S. Kohmoto, and K. Asakawa, "Site-controlled InAs single quantum-dot structures on gaas surfaces patterned by in situ electron-beam lithography," Appl. Phys. Lett. **76**, 167–169 (2000).
16. O. G. Schmidt, *Lateral Aligment of Epitaxial Quantum Dots* (Springer Verlag, 2007).
17. C. Schneider, A. Huggenberger, T. Sunner, T. Heindel, M. Strauss, S. Gopfert, P. Weinmann, S. Reitzenstein, L. Worschech, M. Kamp, S. Höfling, and A. Forchel, "Single site-controlled In(Ga)As/GaAs quantum dots: growth, properties and device integration," Nanotechnology **20**, 434012 (2009).
18. M. H. Baier, S. Watanabe, E. Pelucchi, and E. Kapon, "High uniformity of site-controlled pyramidal quantum dots grown on prepatterned substrates," Appl. Phys. Lett. **84**, 1943–1945 (2004).
19. C. Schneider, T. Heindel, A. Huggenberger, P. Weinmann, C. Kistner, M. Kamp, S. Reitzenstein, S. Höfling, and A. Forchel, "Single photon emission from a site-controlled quantum dot-micropillar cavity system," Appl. Phys. Lett. **94**, 111111 (2009).
20. K. D. Jöns, P. Atkinson, M. Müller, M. Heldmaier, S. M. Ulrich, O. G. Schmidt, and P. Michler, "Triggered indistinguishable single photons with narrow line widths from site-controlled quantum dots," Nano Lett. **13**, 126–130 (2013).
21. G. Juska, V. Dimastrodonato, L. O. Mereni, A. Gocalinska, and E. Pelucchi, "Towards quantum-dot arrays of entangled photon emitters," Nat. Photonics **7**, 527–531 (2013).
22. S. Ates, S. M. Ulrich, S. Reitzenstein, A. Löffler, A. Forchel, and P. Michler, "Post-selected indistinguishable photons from the resonance fluorescence of a single quantum dot in a microcavity," Phys. Rev. Lett. **103**, 167402 (2009).
23. E. Flagg, A. Muller, J. Robertson, S. Founta, D. Deppe, M. Xiao, W. Ma, G. Salamo, and C.-K. Shih, "Resonantly driven coherent oscillations in a solid-state quantum emitter," Nat. Phys. **5**, 203–207 (2009).
24. A. N. Vamivakas, Y. Zhao, C.-Y. Lu, and M. Atatüre, "Spin-resolved quantum-dot resonance fluorescence," Nat. Phys. **5**, 198–202 (2009).
25. P. Royo, R. P. Stanley, and M. Ilegems, "Planar dielectric microcavity light-emitting diodes: analytical analysis of the extraction efficiency," J. Appl. Phys. **90**, 283–293 (2001).
26. O. Gazzano, S. Michaelis de Vasconcellos, C. Arnold, A. Nowak, E. Galopin, I. Sagnes, L. Lanco, A. Lemaître, and P. Senellart, "Bright solid-state sources of indistinguishable single photons," Nat. Commun. **4**, 1425 (2013).
27. S. Maier, P. Gold, A. Forchel, N. Gregersen, J. Mørk, S. Höfling, C. Schneider, and M. Kamp, "Bright single photon source based on self-aligned quantum dot-cavity systems," Opt. Express **22**, 8136–8142 (2014).
28. M. Gschrey, A. Thoma, P. Schnauber, M. Seifried, R. Schmidt, B. Wohlfeil, L. Kruger, J. H. Schulze, T. Heindel, S. Burger, F. Schmidt, A. Strittmatter, S. Rodt, and S. Reitzenstein, "Highly indistinguishable photons from deterministic quantum-dot microlenses utilizing three-dimensional in situ electron-beam lithography," Nat. Commun. **6**, 7662 (2015).
29. L. Sapienza, M. Davanco, A. Badolato, and K. Srinivasan, "Nanoscale optical positioning of single quantum dots for bright and pure single-photon emission," Nat. Commun. **6**, 7833 (2015).
30. F. Albert, S. Stobbe, C. Schneider, T. Heindel, S. Reitzenstein, S. Höfling, P. Lodahl, L. Worschech, and A. Forchel, "Quantum efficiency and oscillator strength of site-controlled InAs quantum dots," Appl. Phys. Lett. **96**, 151102 (2010).
31. D. P. S. McCutcheon and A. Nazir, "Model of the optical emission of a driven semiconductor quantum dot: phonon-enhanced coherent scattering and off-resonant sideband narrowing," Phys. Rev. Lett. **110**, 217401 (2013).
32. A. J. Ramsay, T. M. Godden, S. J. Boyle, E. M. Gauger, A. Nazir, B. W. Lovett, A. M. Fox, and M. S. Skolnick, "Phonon-induced Rabi-frequency renormalization of optically driven single InGaAs/GaAs quantum dots," Phys. Rev. Lett. **105**, 177402 (2010).
33. A. J. Ramsay, A. V. Gopal, E. M. Gauger, A. Nazir, B. W. Lovett, A. M. Fox, and M. S. Skolnick, "Damping of exciton Rabi rotations by acoustic phonons in optically excited InGaAs/GaAs quantum dots," Phys. Rev. Lett. **104**, 017402 (2010).
34. D. P. S. McCutcheon and A. Nazir, "Quantum dot Rabi rotations beyond the weak exciton-phonon coupling regime," New J. Phys. **12**, 113042 (2010).
35. Y.-J. Wei, Y. He, Y.-M. He, C.-Y. Lu, J.-W. Pan, C. Schneider, M. Kamp, S. Höfling, D. P. S. McCutcheon, and A. Nazir, "Temperature-dependent Mollow triplet spectra from a single quantum dot: Rabi frequency renormalization and sideband linewidth insensitivity," Phys. Rev. Lett. **113**, 097401 (2014).
36. H. J. Carmichael, *Statistical Methods in Quantum Optics* (Springer, 1998).
37. D. P. S. McCutcheon, "Optical signatures of non-Markovian behaviour in open quantum systems," arXiv:1504.05970 (2015).
38. P. Michler, A. Imamoglu, A. Kiraz, C. Becher, M. Mason, P. Carson, G. Strouse, S. Buratto, W. Schoenfeld, and P. Petroff, "Nonclassical radiation from a single quantum dot," Phys. Status Solidi B **229**, 399–405 (2002).
39. J. Johansen, S. Stobbe, I. S. Nikolaev, T. Lund-Hansen, P. T. Kristensen, J. M. Hvam, W. L. Vos, and P. Lodahl, "Size dependence of the wavefunction of self-assembled InAs quantum dots from time-resolved optical measurements," Phys. Rev. B **77**, 073303 (2008).
40. A. Ulhaq, S. Weiler, C. Roy, S. M. Ulrich, M. Jetter, S. Hughes, and P. Michler, "Detuning-dependent Mollow triplet of a coherently-driven single quantum dot," Opt. Express **21**, 4382–4395 (2013).
41. A. Musiał, P. Gold, J. Andrzejewski, A. Löffler, J. Misiewicz, S. Höfling, A. Forchel, M. Kamp, G. Sek, and S. Reitzenstein, "Toward weak confinement regime in epitaxial nanostructures: interdependence of spatial character of quantum confinement and wave function extension in large and elongated quantum dots," Phys. Rev. B **90**, 045430 (2014).
42. D. Press, T. D. Ladd, B. Zhang, and Y. Yamamoto, "Complete quantum control of a single quantum dot spin using ultrafast optical pulses," Nature **456**, 218–221 (2008).